RAPID COMMUNICATIONS

PHYSICAL REVIEW MATERIALS **1**, 061401(R) (2017)

Mode-dependent damping in metallic antiferromagnets due to intersublattice spin pumping

Qian Liu,[1] H. Y. Yuan,[2] Ke Xia,[1,3] and Zhe Yuan[1,*]

[1]*The Center for Advanced Quantum Studies and Department of Physics, Beijing Normal University, 100875 Beijing, China*

[2]*Department of Physics, South University of Science and Technology of China, Shenzhen, Guangdong 518055, China*

[3]*Synergetic Innovation Center for Quantum Effects and Applications (SICQEA), Hunan Normal University, Changsha 410081, China*

(Received 26 April 2017; published 13 November 2017)

Damping in magnetization dynamics characterizes the dissipation of magnetic energy and is essential for improving the performance of spintronics-based devices. While the damping of ferromagnets has been well studied and can be artificially controlled in practice, the damping parameters of antiferromagnetic materials are nevertheless little known for their physical mechanisms or numerical values. Here we calculate the damping parameters in antiferromagnetic dynamics using the generalized scattering theory of magnetization dissipation combined with the first-principles transport computation. For the PtMn, IrMn, PdMn, and FeMn metallic antiferromagnets, the damping coefficient associated with the motion of magnetization (α_m) is 1–3 orders of magnitude larger than the other damping coefficient associated with the variation of the Néel order (α_n), in sharp contrast to the assumptions made in the literature.

DOI: 10.1103/PhysRevMaterials.1.061401

Damping describes the process of energy dissipation in dynamics and determines the time scale for a nonequilibrium system relaxing back to its equilibrium state. For magnetization dynamics of ferromagnets (FMs), the damping is characterized by a phenomenological dissipative torque exerted on the precessing magnetization [1]. The magnitude of this torque, which depends on material, temperature, and magnetic configurations, has been well studied in experiment [2–10] and theory [11–16].

Recently, the magnetization dynamics of antiferromagnets (AFMs) [17–20], especially those controlled by an electric or spin current [21–32], has attracted lots of attention in the process of searching for high-performance spintronic devices. However, the understanding of AFM dynamics, in particular the damping mechanism and magnitude in real materials, is quite limited. The magnetization dynamics of a collinear AFM can be described by two coupled Landau-Lifshitz-Gilbert (LLG) equations corresponding to the precessional motion of the two sublattices, respectively [33], i.e. ($i = 1,2$),

$$\dot{\mathbf{m}}_i = -\gamma \mathbf{m}_i \times \mathbf{h}_i + \alpha_i \mathbf{m}_i \times \dot{\mathbf{m}}_i, \qquad (1)$$

where γ is the gyromagnetic ratio, $\mathbf{m}_i$ is the magnetization direction on the ith sublattice, and $\dot{\mathbf{m}}_i = \partial_t \mathbf{m}_i$. $\mathbf{h}_i$ is the effective magnetic field on $\mathbf{m}_i$, which contains the anisotropy field, the external field, and the exchange field arising from the magnetization on both sublattices. The last contribution to $\mathbf{h}_i$ makes the dynamic equation of one sublattice coupled to the equation of the other one. Specifically, if the free energy of the AFM is given by the following form, $\mathcal{F}[\mathbf{m}_1,\mathbf{m}_2] \equiv \mu_0 M_s V \mathcal{E}[\mathbf{m}_1,\mathbf{m}_2]$, with the permeability of vacuum μ_0, the magnetization on each sublattice M_s, and the volume of the AFM V, one has $\mathbf{h}_i = -\delta\mathcal{E}/\delta\mathbf{m}_i$. α_i in Eq. (1) is the damping parameter representing the dissipation rate of the magnetization $\mathbf{m}_i$. Due to the sublattice permutation symmetry, the damping magnitudes of the two sublattices should be equal. This approach has been used to investigate the AFM resonance [33,34], temperature-gradient-induced domain wall (DW) motion [35], and spin-transfer torques in an AFM|FM bilayer [36].

An alternative way to deal with the AFM dynamics is introducing the net magnetization $\mathbf{m} \equiv \mathbf{m}_1 + \mathbf{m}_2$ and the Néel order $\mathbf{n} \equiv \mathbf{m}_1 - \mathbf{m}_2$ so that the precessional motion of $\mathbf{m}$ and $\mathbf{n}$ can be derived from the Lagrangian equation [26]. The damping effect is then included artificially with two parameters α_m and α_n that characterize the dissipation rate of $\mathbf{m}$ and $\mathbf{n}$, respectively. This approach is widely used to investigate the spin superfluid in an AFM insulator [37,38], an AFM nano-oscillator [39], and DW motion induced by an electrical current [26,40], spin waves [41], and spin-orbit torques [42,43]. Using the above definitions of $\mathbf{m}$ and $\mathbf{n}$, one can reformulate Eq. (1) and derive the following dynamic equations:

$$\dot{\mathbf{n}} = (\gamma \mathbf{h}_m - \alpha_m \dot{\mathbf{m}}) \times \mathbf{n} + (\gamma \mathbf{h}_n - \alpha_n \dot{\mathbf{n}}) \times \mathbf{m}, \qquad (2)$$

$$\dot{\mathbf{m}} = (\gamma \mathbf{h}_m - \alpha_m \dot{\mathbf{m}}) \times \mathbf{m} + (\gamma \mathbf{h}_n - \alpha_n \dot{\mathbf{n}}) \times \mathbf{n}, \qquad (3)$$

where $\mathbf{h}_n$ and $\mathbf{h}_m$ are the effective magnetic fields exerted on $\mathbf{n}$ and $\mathbf{m}$, respectively. They can also be written as the functional derivative of the free energy [26,41], i.e., $\mathbf{h}_n = -\delta\mathcal{E}/\delta\mathbf{n}$ and $\mathbf{h}_m = -\delta\mathcal{E}/\delta\mathbf{m}$. The damping parameters in Eqs. (1)–(3) have the relation $\alpha_n = \alpha_m = \alpha_1/2 = \alpha_2/2$ [36]. Indeed, the assumption $\alpha_m = \alpha_n$ is commonly adopted in the theoretical study of AFM dynamics with only a few exceptions, where α_m is ignored in the current-induced skyrmion motion in AFM materials [44] and the magnon-driven DW motion [45]. However, the underlying damping mechanism of an AFM and the relation between α_m and α_n have not been fully justified yet [46,47].

In this paper, we generalize the scattering theory of magnetization dissipation in FMs [48] to AFMs and calculate the damping parameters from first principles for metallic AFMs PtMn, IrMn, PdMn, and FeMn. The damping coefficients in an AFM are found to be strongly mode dependent, with α_m up to 3 orders of magnitude larger than α_n. By analyzing the dependence of damping on the disorder and spin-orbit coupling

*Corresponding author: zyuan@bnu.edu.cn

(SOC), we demonstrate that α_n arises from SOC in analog to the Gilbert damping in FMs, while α_m is dominated by the spin pumping effect between sublattices.

Theory. In analog to the scattering theory of magnetization dissipation in FMs [48], the damping parameters in AFMs, α_n and α_m, can be expressed in terms of the scattering matrix. Following the previous definition of the free energy, the energy dissipation rate of an AFM reads

$$\dot{E} = -\mu_0 M_s V \dot{\mathcal{E}} = \mu_0 M_s V \left(-\frac{\delta \mathcal{E}}{\delta \mathbf{m}} \cdot \dot{\mathbf{m}} - \frac{\delta \mathcal{E}}{\delta \mathbf{n}} \cdot \dot{\mathbf{n}} \right) = \mu_0 M_s V (\mathbf{h}_m \cdot \dot{\mathbf{m}} + \mathbf{h}_n \cdot \dot{\mathbf{n}}). \quad (4)$$

By replacing the effective fields $\mathbf{h}_m$ and $\mathbf{h}_n$ by the time derivative of magnetization order and Néel order using Eqs. (2) and (3), one arrives at [49]

$$\dot{E} = \frac{\mu_0 M_s V}{\gamma} (\alpha_n \dot{\mathbf{n}}^2 + \alpha_m \dot{\mathbf{m}}^2). \quad (5)$$

If we place an AFM between two semi-infinite nonmagnetic metals, the propagating electronic states coming from the metallic leads are partly reflected and transmitted. The probability amplitudes of the reflection and transmission form the so-called scattering matrix **S** [50]. For such a scattering structure with only the order parameter **n** of the AFM varying in time (see the insets of Fig. 1), the energy loss that is pumped into the reservoir is given by

$$\dot{E} = \frac{\hbar}{4\pi} \mathrm{Tr}(\dot{\mathbf{S}} \dot{\mathbf{S}}^\dagger) = \frac{\hbar}{4\pi} \mathrm{Tr}\left(\frac{\partial \mathbf{S}}{\partial \mathbf{n}} \frac{\partial \mathbf{S}^\dagger}{\partial \mathbf{n}} \right) \dot{\mathbf{n}}^2 \equiv D_n \dot{\mathbf{n}}^2. \quad (6)$$

Here we define $D_n \equiv (\hbar/4\pi)\mathrm{Tr}[(\partial \mathbf{S}/\partial \mathbf{n})(\partial \mathbf{S}^\dagger/\partial \mathbf{n})]$. Comparing Eqs. (5) and (6), we obtain

$$D_n = \frac{\mu_0 M_s A}{\gamma} \alpha_n L, \quad (7)$$

where we replace the volume V by the product of the cross-sectional area A and the length L of the AFM. We can express α_m in the same manner,

$$D_m = \frac{\mu_0 M_s A}{\gamma} \alpha_m L, \quad (8)$$

with $D_m \equiv (\hbar/4\pi)\mathrm{Tr}[(\partial \mathbf{S}/\partial \mathbf{m})(\partial \mathbf{S}^\dagger/\partial \mathbf{m})]$. Using Eqs. (7) and (8), we calculate the energy dissipation as a function of the length L and extract the damping parameters $\alpha_{n(m)}$ via a linear-least-squares fitting. Note that the above formalism can be generalized to include noncollinear AFM, such as DWs in AFMs, by introducing the position-dependent order parameters $\mathbf{n}(\mathbf{r})$ and $\mathbf{m}(\mathbf{r})$. It can also be extended for the AFMs containing more than two sublattices, which may not be collinear with one another [51]. For the latter case, one has to redefine the proper order parameters instead of **n** and **m** [52].

First-principles calculations. The above formalism is implemented using the first-principles scattering calculation and is applied here in studying the damping of metallic AFMs including PtMn, IrMn, PdMn, and FeMn. The lattice constants and magnetic configurations are the same as in the reported first-principles calculations [53]. Here we take tetragonal PtMn as an example to illustrate the computational details. A finite thickness (L) of PtMn is connected to two semi-infinite Au leads along (001) direction. The lattice constant of Au is made to match that of the a axis of PtMn. The electronic structures are obtained self-consistently within the density functional theory implemented with a minimal basis of the tight-binding linear muffin-tin orbitals (TB LMTOs) [54]. The magnetic moment of every Mn atom is 3.65 μ_B and Pt atoms are not magnetized.

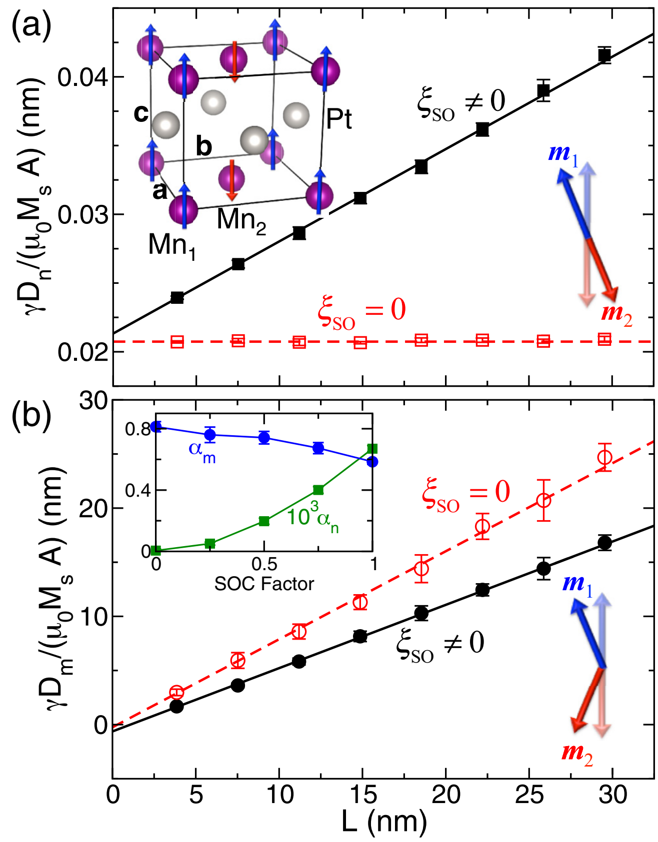

FIG. 1. Calculated energy dissipation rate as a function of the length of PtMn due to variation of the order parameters **n** (a) and **m** (b). A is the cross-sectional area of the lateral supercell. Arrows in each panel illustrate the dynamical modes of the order parameters. The empty symbols are calculated without spin-orbit interaction. The inset of panel (a) shows the atomic structure of PtMn with collinear AFM order. The inset in (b) shows calculated α_n and α_m as a function of the scaled SOC strength. The factor 1 corresponds to the real SOC strength that is determined by the derivative of the self-consistent potentials.

To evaluate α_n and α_m, we first construct a lateral 10×10 supercell including 100 atoms per atomic layer in the scattering region, where the atoms are randomly displaced from their equilibrium lattice sites using a Gaussian distribution with the rms displacement Δ [15,55]. The value of Δ is chosen to reproduce typical experimental resistivity of the corresponding bulk AFM. The scattering matrix **S** is obtained using a first-principles "wave-function matching" scheme that is also implemented with TB LMTOs [56], and its derivative is obtained by the finite-difference method [49].

Figure 1(a) shows the calculated energy-pumping rate D_n of PtMn as a function of L for **n** along the c axis with $\Delta/a = 0.049$. The total pumping rate (solid symbols) increases linearly with increasing the volume of the AFM. A linear-least-squares fitting yields $\alpha_n = (0.67 \pm 0.02) \times 10^{-3}$, as plotted by the solid line. The finite intercept of the solid line corresponds to the interface-enhanced energy dissipation, which is essentially the spin pumping effect at the AFM|Au interface [57,58]. The Néel-order-induced damping α_n completely results from SOC. If we artificially turn SOC off, the calculated pumping rate is independent of the volume of the AFM, indicating $\alpha_n = 0$. This is because the spin space is decoupled from the real space without SOC and the energy is then invariant with respect to the direction of $\mathbf{n}$. The spin-pumping effect is nearly unchanged by the SOC.

The energy-pumping rate D_m of PtMn with $\mathbf{n}$ along the c axis is plotted in Fig. 1(b), where we find three important features: (1) The extracted value of $\alpha_m = 0.59 \pm 0.02$, which is nearly 1000 times larger than α_n. (2) Turning SOC off only slightly increases the calculated α_m, indicating that SOC is not the main dissipative mechanism of α_m. The difference between the solid and empty circles in Fig. 1(b) can be attributed to the SOC-induced variation of electronic structure near the Fermi level. To see more clearly the different influence of SOC on α_m and α_n, we plot in the inset of Fig. 1(b) the calculated damping parameters as a function of SOC strength. Indeed, as the SOC strength ξ_{SO} is artificially tuned from its real value to zero, α_n decreases dramatically and tends to vanish at $\xi_{SO} = 0$, while α_m is less sensitive to ξ_{SO} than α_n. (3) The intercepts of the solid and dashed lines are both vanishingly small, indicating that this specific mode does not pump spin current into the nonmagnetic leads. The pumped spin current from an AFM generally reads $\mathbf{I}_s^{\text{pump}} \propto \mathbf{n} \times \dot{\mathbf{n}} + \mathbf{m} \times \dot{\mathbf{m}}$ [58]. For the mode depicted in Fig. 1(b), one has $\dot{\mathbf{n}} = 0$ and $\dot{\mathbf{m}} \| \mathbf{m}$ such that $\mathbf{I}_s^{\text{pump}} = 0$.

To explore the disorder dependence of the damping parameters α_n and α_m, we further perform the calculation by varying the rms of atomic displacements Δ. Figure 2(a) shows that the calculated resistivity increases monotonically with increasing Δ. The resistivity ρ_c with $\mathbf{n}$ along the c axis is lower than ρ_a with $\mathbf{n}$ along the a axis. The anisotropic magnetoresistance (AMR) defined by $(\rho_a - \rho_c)/\rho_c$ is about 10%, which slightly decreases with increasing Δ, as plotted in the inset of Fig. 2(a). The large AMR in PtMn is useful for experimental detection of the Néel order. The calculated AMR seems to be an order of magnitude larger than the reported values in literature [59–61]. We may attribute the difference to the surface scattering in thin-film samples and other types of disorder that have been found to decrease the AMR of ferromagnetic metals and alloys [62].

α_n of PtMn plotted in Fig. 2(b) is of the order of 10^{-3}, which is comparable with the magnitude of the Gilbert damping of ferromagnetic transition metals [2–4,15]. For $\mathbf{n}$ along the a axis, α_n shows a weak nonmonotonic dependence on disorder, while α_n for $\mathbf{n}$ along the c axis increases monotonically. With the relativistic SOC, the electronic structure of an AFM depends on the orientation of $\mathbf{n}$. When $\mathbf{n}$ varies in time, the occupied energy bands may be lifted above the Fermi level. Then a longer relaxation time (weaker disorder) gives rise to a larger energy dissipation, corresponding to the increase in α_n with decreasing Δ at small Δ. It is analogous to the intraband transitions accounting for the conductivitylike behavior of Gilbert damping at low temperature in the torque-correlation

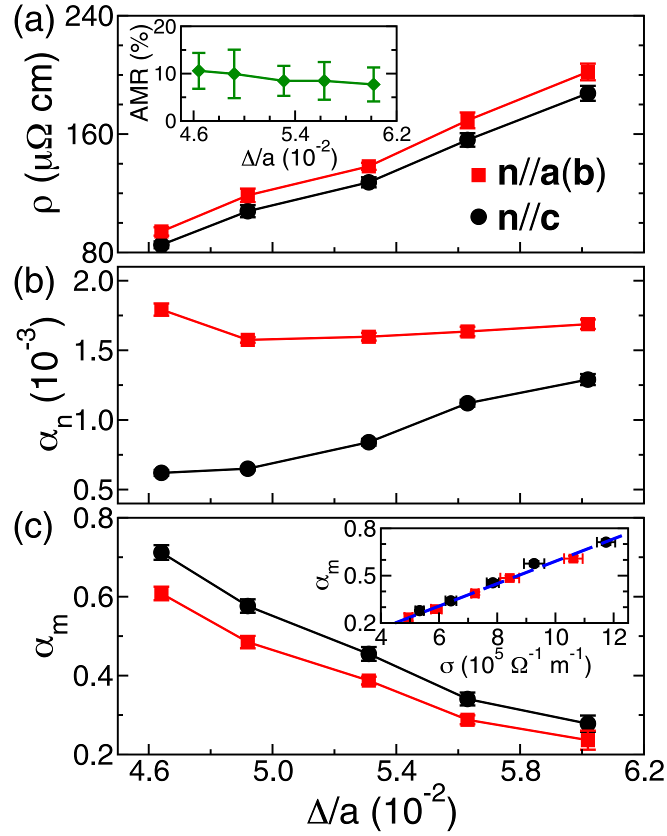

FIG. 2. Calculated resistivity (a) and damping parameters α_n (b) and α_m (c) of PtMn as a function of the rms of atomic displacements. The red squares and black circles are calculated with $\mathbf{n}$ along the a and c axis, respectively. The inset of (a) shows the calculated AMR. α_m is replotted as a function of conductivity in the inset of (c). The blue dashed line illustrates the linear dependence.

model [11,12]. Sufficiently strong disorder renders the system isotropic, and the variation of $\mathbf{n}$ does not lead to electronic excitation, but scattering of conduction electrons by disorder still dissipates energy into the lattice through SOC. The higher the scattering rate, the larger the energy dissipation rate corresponding to the contribution of the interband transitions [11,12]. Therefore, α_n shares the same physical origin as the Gilbert damping of metallic FMs.

The value of α_m is about 3 orders of magnitude larger than α_n, and it decreases monotonically with increasing the structural disorder, as shown in Fig. 2(c). This remarkable difference can be attributed to the energy involved in the dynamical motion of $\mathbf{m}$ and $\mathbf{n}$. While the precession of $\mathbf{n}$ only changes the magnetic anisotropy energy in an AFM, the variation of $\mathbf{m}$ changes the exchange energy that is in magnitude much larger than the magnetic anisotropy energy.

Physically, α_m can be understood in terms of spin pumping [63,64] between the two sublattices of an AFM. The sublattice $\mathbf{m}_2$ pumps a spin current that can be absorbed by $\mathbf{m}_1$, resulting in a damping torque exerted on $\mathbf{m}_1$ as $\alpha' \mathbf{m}_1 \times [\mathbf{m}_1 \times (\mathbf{m}_2 \times \dot{\mathbf{m}}_2)]$. Here α' is a dimensionless parameter to describe the strength of the spin pumping. This torque can be simplified to be $\alpha' \mathbf{m}_1 \times \dot{\mathbf{m}}_2$ by neglecting the higher-order terms of the total magnetization $\mathbf{m}$. In addition, the spin pumping by $\mathbf{m}_1$

TABLE I. Calculated resistivity and damping parameters for the Néel order **n** along the a and c axis.

AFM	**n**	ρ ($\mu\Omega$ cm)	α_n (10^{-3})	α_m
PtMn	a axis	119 ± 5	1.60 ± 0.02	0.49 ± 0.02
	c axis	108 ± 4	0.67 ± 0.02	0.59 ± 0.02
IrMn	a axis	116 ± 2	10.5 ± 0.2	0.10 ± 0.01
	c axis	116 ± 2	10.2 ± 0.3	0.10 ± 0.01
PdMn	a axis	120 ± 8	0.16 ± 0.02	1.1 ± 0.10
	c axis	121 ± 8	1.30 ± 0.10	1.30 ± 0.10
FeMn	a axis	90 ± 1	0.76 ± 0.04	0.38 ± 0.01
	c axis	91 ± 1	0.82 ± 0.03	0.38 ± 0.01

also contributes to the damping of the sublattice $\mathbf{m}_1$ that is equivalent to a torque $\alpha' \mathbf{m}_1 \times \dot{\mathbf{m}}_1$ exerted on $\mathbf{m}_1$. Taking the intersublattice spin pumping into account, we are able to derive Eqs. (2) and (3) and obtain the damping parameters $\alpha_n = \alpha_0/2$ and $\alpha_m = (\alpha_0 + 2\alpha')/2$ [49]. Here α_0 is the intrinsic damping due to SOC for each sublattice. It is worth noting that the spin pumping strength within a metal is proportional to its conductivity [65–67]. We replot α_m as a function of conductivity in the inset of Fig. 2(c), where a general linear dependence is seen for **n** along both the a axis and c axis.

We list in Table I the calculated ρ, α_n, and α_m for typical metallic AFMs including PtMn, IrMn, PdMn, and FeMn. For IrMn, α_m is only 10 times larger than α_n, while α_m of the other three materials are about 3 orders of magnitude larger than their α_n.

Antiferromagnetic resonance. Keffer and Kittel formulated antiferromagnetic resonance (AFMR) without damping [33] and determined the resonant frequencies that depend on the external field $H_{\rm ext}$, exchange field H_E, and anisotropy field H_A, $\omega_{\rm res} = \gamma[H_{\rm ext} \pm \sqrt{H_A(2H_E + H_A)}]$. Here we follow their approach, in which $H_{\rm ext}$ is applied along the easy axis and the transverse components of $\mathbf{m}_1$ and $\mathbf{m}_2$ are supposed to be small. Taking both the intrinsic damping due to SOC and spin pumping between the two sublattices into account, we solve the dynamical equations of AFMR and find the frequency-dependent susceptibility $\boldsymbol{\chi}(\omega)$ that is defined by $\mathbf{n}_\perp(\omega) = \boldsymbol{\chi}(\omega) \cdot \mathbf{h}_\perp(\omega)$. Here $\mathbf{n}_\perp$ and $\mathbf{h}_\perp$ are the transverse components of the Néel order and microwave field, respectively. The imaginary part of the diagonal element of $\boldsymbol{\chi}(\omega)$ with $H_{\rm ext} = 20$ kOe is plotted in the inset of Fig. 3, where two resonance modes can be identified. The precessional modes for the positive (ω_R) and negative frequency (ω_L) are schematically depicted in Fig. 3. The linewidth of the AFMR $\Delta\omega$ can be determined from the imaginary part of the (complex) eigenfrequency [68] by solving $\det|\boldsymbol{\chi}^{-1}(\omega)| = 0$ and is plotted in Fig. 3 as a function of $H_{\rm ext}$. Without $H_{\rm ext}$, the two modes have the same linewidth. A finite external field increases the linewidth of ω_R and decreases that of ω_L, both linearly. By including the spin pumping between two sublattices, both the linewidth at $H_{\rm ext} = 0$ and the slope of $\Delta\omega$ as a function of $H_{\rm ext}$ increase by

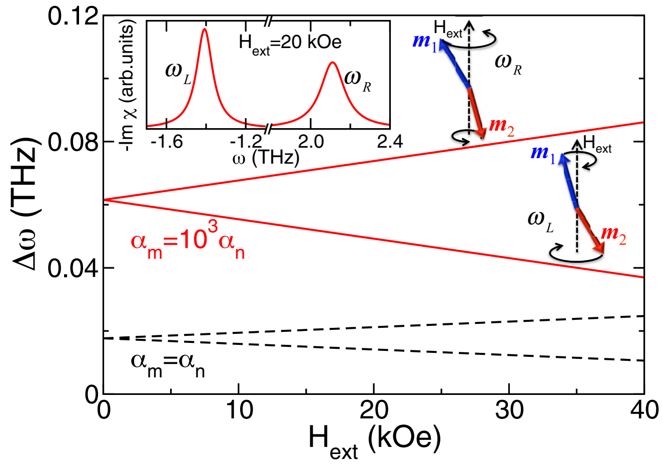

FIG. 3. Linewidth of AFMR as a function of the external magnetic field. The black dashed lines and red solid lines are calculated with $\alpha_m = \alpha_n$ and $\alpha_m = 10^3\alpha_n$, respectively. Inset: The imaginary part of susceptibility as a function of the frequency for the external magnetic field $H_{\rm ext} = 20$ kOe and $\alpha_m = 10^3\alpha_n$. The cartoons illustrate the corresponding dynamical modes. Here we use $H_E = 10^3$ kOe, $H_A = 5$ kOe, and $\alpha_n = 0.001$.

a factor of about 3.5, which indicates that the spin-pumping effect between the two sublattices plays an important role in the magnetization dynamics of metallic AFMs.

Conclusions. We have generalized the scattering theory of magnetization dissipation in FMs to be applicable for AFMs. Using first-principles scattering calculation, we find the damping parameter accompanying the motion of magnetization (α_m) is generally much larger than that associated with the motion of the Néel order (α_n) in the metallic AFMs PtMn, IrMn, PdMn, and FeMn. While α_n arises from the spin-orbit interaction, α_m is mainly contributed by the spin pumping between the two sublattices in an AFM via exchange interaction. Taking AFMR as an example, we demonstrate that the linewidth can be significantly enhanced by the giant value of α_m. Our findings suggest that the magnetization dynamics of AFMs shall be revisited with the damping effect properly included.

Note added in proof. Recently, we became aware of a preprint [69], in which the intersublattice spin pumping is also found to play an important role in the spin transport across an AFM|NM or ferrimagnet|NM interface.

Acknowledgments. We would like to thank the helpful discussions with X. R. Wang. This work was financially supported by the National Key Research and Development Program of China (Contract No. 2017YFA0303300) and the National Natural Science Foundation of China (Grants No. 61774018, No. 61704071, No. 61774017, No. 11734004, and No. 21421003). Z.Y. acknowledges the Recruitment Program of Global Youth Experts.

Q.L. and H.Y.Y. contributed equally to this work.

[1] T. L. Gilbert, A phenomenological theory of damping in ferromagnetic materials, IEEE Trans. Magn. **40**, 3443 (2004).

[2] B. Heinrich and Z. Frait, Temperature dependence of the FMR linewidth of iron single-crystal platelets, Phys. Status Solidi B **16**, K11 (1966).

[3] S. M. Bhagat and P. Lubitz, Temperature variation of ferromagnetic relaxation in the 3d transition metals, Phys. Rev. B **10**, 179 (1974).

[4] B. Heinrich, D. J. Meredith, and J. F. Cochran, Wave number and temperature-dependent Landau-Lifshitz damping in nickel, J. Appl. Phys. **50**, 7726 (1979).

[5] S. Mizukami, Y. Ando, and T. Miyazaki, The study on ferromagnetic resonance linewidth for NM/80NiFe/NM(NM=Cu, Ta, Pd and Pt) films, Jpn. J. Appl. Phys. **40**, 580 (2001).

[6] S. Mizukami, Y. Ando, and T. Miyazaki, Ferromagnetic resonance linewidth for NM/80NiFe/NM films (NM=Cu, Ta, Pd and Pt), J. Magn. Magn. Mater. **226**, 1640 (2001).

[7] S. Ingvarsson, L. Ritchie, X. Y. Liu, G. Xiao, J. C. Slonczewski, P. L. Trouilloud, and R. H. Koch, Role of electron scattering in the magnetization relaxation of thin $Ni_{81}Fe_{19}$ films, Phys. Rev. B **66**, 214416 (2002).

[8] P. Lubitz, S. F. Cheng, and F. J. Rachford, Increase of magnetic damping in thin polycrystalline Fe films induced by Cu/Fe overlayers, J. Appl. Phys. **93**, 8283 (2003).

[9] S. Yakata, Y. Ando, T. Miyazaki, and S. Mizukami, Temperature dependences of spin-diffusion lengths of Cu and Ru layers, Jpn. J. Appl. Phys. **45**, 3892 (2006).

[10] T. Weindler, H. G. Bauer, R. Islinger, B. Boehm, J.-Y. Chauleau, and C. H. Back, Magnetic Damping: Domain Wall Dynamics Versus Local Ferromagnetic Resonance, Phys. Rev. Lett. **113**, 237204 (2014).

[11] V. Kamberský, On ferromagnetic resonance damping in metals, Czech. J. Phys. **26**, 1366 (1976); Spin-orbital Gilbert damping in common magnetic metals, Phys. Rev. B **76**, 134416 (2007).

[12] K. Gilmore, Y. U. Idzerda, and M. D. Stiles, Identification of the Dominant Precession-Damping Mechanism in Fe, Co, and Ni by First-Principles Calculations, Phys. Rev. Lett. **99**, 027204 (2007); K. Gilmore, M. D. Stiles, J. Seib, D. Steiauf, and M. Fähnle, Anisotropic damping of the magnetization dynamics in Ni, Co, and Fe, Phys. Rev. B **81**, 174414 (2010).

[13] A. A. Starikov, P. J. Kelly, A. Brataas, Y. Tserkovnyak, and G. E. W. Bauer, Unified First-Principles Study of Gilbert Damping, Spin-Flip Diffusion, and Resistivity in Transition Metal Alloys, Phys. Rev. Lett. **105**, 236601 (2010).

[14] H. Ebert, S. Mankovsky, D. Ködderitzsch, and P. J. Kelly, *Ab Initio* Calculation of the Gilbert Damping Parameter via Linear Response Formalism, Phys. Rev. Lett. **107**, 066603 (2011).

[15] Y. Liu, A. A. Starikov, Z. Yuan, and P. J. Kelly, First-principles calculations of magnetization relaxation in pure Fe, Co, and Ni with frozen thermal lattice disorder, Phys. Rev. B **84**, 014412 (2011).

[16] H.-M. Tang and K. Xia, Gilbert Damping Parameter in MgO-Based Magnetic Tunnel Junctions from First Principles, Phys. Rev. Appl. **7**, 034004 (2017).

[17] A. V. Kimel, A. Kirilyuk, A. Tsvetkov, R. V. Pisarev, and Th. Rasing, Laser-induced ultrafast spin reorientation in the antiferromagnet $TmFeO_3$, Nature (London) **429**, 850 (2004).

[18] A. H. MacDonald and M. Tsoi, Antiferromagnetic metal spintronics, Philos. Trans. R. Soc. A **369**, 3098 (2011).

[19] X. Marti, I. Fina, C. Frontera, J. Liu, P. Wadley, Q. He, R. J. Paull, J. D. Clarkson, J. Kudrnovský, I. Turek, J. Kuneš, D. Yi, J-H. Chu, C. T. Nelson, L. You, E. Arenholz, S. Salahuddin, J. Fontcuberta, T. Jungwirth, and R. Ramesh, Room-temperature antiferromagnetic memory resistor, Nat. Mater. **13**, 367 (2014).

[20] T. Jungwirth, X. Marti, P. Wadley, and J. Wunderlich, Antiferromagnetic spintronics, Nat. Nanotechnol. **11**, 231 (2016).

[21] A. S. Núñez, R. A. Duine, P. Haney, and A. H. MacDonald, Theory of spin torques and giant magnetoresistance in antiferromagnetic metals, Phys. Rev. B **73**, 214426 (2006).

[22] P. M. Haney, D. Waldron, R. A. Duine, A. S. Núñez, H. Guo, and A. H. MacDonald, *Ab initio* giant magnetoresistance and current-induced torques in Cr/Au/Cr multilayers, Phys. Rev. B **75**, 174428 (2007).

[23] Y. Xu, S. Wang, and K. Xia, Spin-Transfer Torques in Antiferromagnetic Metals from First Principles, Phys. Rev. Lett. **100**, 226602 (2008).

[24] P. M. Haney and A. H. MacDonald, Current-Induced Torques Due to Compensated Antiferromagnets, Phys. Rev. Lett. **100**, 196801 (2008).

[25] A. C. Swaving and R. A. Duine, Current-induced torques in continuous antiferromagnetic textures, Phys. Rev. B **83**, 054428 (2011).

[26] K. M. D. Hals, Y. Tserkovnyak, and A. Brataas, Phenomenology of Current-Induced Dynamics in Antiferromagnets, Phys. Rev. Lett. **106**, 107206 (2011).

[27] J. Železný, H. Gao, K. Výborný, J. Zemen, J. Mašek, A. Manchon, J. Wunderlich, J. Sinova, and T. Jungwirth, Relativistic Néel-order Fields Induced by Electrical Current in Antiferromagnets, Phys. Rev. Lett. **113**, 157201 (2014).

[28] D. Qu, S. Y. Huang, and C. L. Chien, Inverse spin Hall effect in Cr: Independence of antiferromagnetic ordering, Phys. Rev. B **92**, 020418 (2015).

[29] X. Zhang, Y. Zhou, and M. Ezawa, Antiferromagnetic skyrmion: Stability, creation and manipulation, Sci. Rep. **6**, 24795 (2016).

[30] J. Barker and O. A. Tretiakov, Static and Dynamical Properties of Antiferromagnetic Skyrmions in the Presence of Applied Current and Temperature, Phys. Rev. Lett. **116**, 147203 (2016).

[31] S. Fukami, C. Zhang, S. Dutta Gupta, A. Kurenkov, and H. Ohno, Magnetization switching by spin-orbit torque in an antiferromagnet-ferromagnet bilayer system, Nat. Mater. **15**, 535 (2016).

[32] P. Wadley, B. Howells, J. Železný, C. Andrews, V. Hills, R. P. Campion, V. Novák, K. Olejník, F. Maccherozzi, S. S. Dhesi, S. Y. Martin, T. Wagner, J. Wunderlich, F. Freimuth, Y. Mokrousov, J. Kuneš, J. S. Chauhan, M. J. Grzybowski, A. W. Rushforth, K. W. Edmonds, B. L. Gallagher, and T. Jungwirth, Electrical switching of an antiferromagnet, Science **351**, 587 (2016).

[33] F. Keffer and C. Kittel, Theory of antiferromagnetic resonance, Phys. Rev. **85**, 329 (1952).

[34] P. Ross, M. Schreier, J. Lotze, H. Huebl, R. Gross, and S. T. B. Goennenwein, Antiferromagentic resonance detected by direct current voltages in MnF_2/Pt bilayers, J. Appl. Phys. **118**, 233907 (2015).

[35] S. Selzer, U. Atxitia, U. Ritzmann, D. Hinzke, and U. Nowak, Inertia-Free Thermally Driven Domain-Wall Motion in Antiferromagnets, Phys. Rev. Lett. **117**, 107201 (2016).

[36] H. V. Gomonay and V. M. Loktev, Spin transfer and current-induced switching in antiferromagnets, Phys. Rev. B **81**, 144427 (2010).

[37] B. I. Halperin and P. C. Hohenberg, Hydrodynamic theory of spin waves, Phys. Rev. **188**, 898 (1969).

[38] S. Takei, B. I. Halperin, A. Yacoby, and Y. Tserkovnyak, Superfluid spin transport through antiferromagnetic insulators, Phys. Rev. B **90**, 094408 (2014).
[39] R. Cheng, D. Xiao, and A. Brataas, Terahertz Antiferromagnetic Spin Hall Nano-Oscillator, Phys. Rev. Lett. **116**, 207603 (2016).
[40] E. G. Tveten, A. Qaiumzadeh, O. A. Tretiakov, and A. Brataas, Staggered Dynamics in Antiferromagnets by Collective Coordinates, Phys. Rev. Lett. **110**, 127208 (2013).
[41] E. G. Tveten, A. Qaiumzadeh, and A. Brataas, Antiferromagnetic Domain Wall Motion Induced by Spin Waves, Phys. Rev. Lett. **112**, 147204 (2014).
[42] O. Gomonay, T. Jungwirth, and J. Sinova, High Antiferromagnetic Domain Wall Velocity Induced by Néel Spin-Orbit Torques, Phys. Rev. Lett. **117**, 017202 (2016).
[43] T. Shiino, S.-H. Oh, P. M. Haney, S.-W. Lee, G. Go, B.-G. Park, and K.-J. Lee, Antiferromagnetic Domain Wall Motion Driven by Spin-Orbit Torques, Phys. Rev. Lett. **117**, 087203 (2016).
[44] H. Velkov, O. Gomonay, M. Beens, G. Schwiete, A. Brataas, J. Sinova, and R. A. Duine, Phenomenology of current-induced skyrmion motion in antiferromagnets, New J. Phys. **18**, 075016 (2016).
[45] S. K. Kim, Y. Tserkovnyak, and O. Tchernyshyov, Propulsion of a domain wall in an antiferromagnet by magnons, Phys. Rev. B **90**, 104406 (2014).
[46] E. V. Gomonay and V. M. Loktev, Spintronics of antiferromagnetic systems (review article), Low Temp. Phys. **40**, 17 (2014).
[47] U. Atxitia, D. Hinzke, and U. Nowak, Fundamentals and applications of the Landau-Lifshitz-Bloch equation, J. Phys. D: Appl. Phys. **50**, 033003 (2017).
[48] A. Brataas, Y. Tserkovnyak, and G. E. W. Bauer, Scattering Theory of Gilbert Damping, Phys. Rev. Lett. **101**, 037207 (2008); Magnetization dissipation in ferromagnets from scattering theory, Phys. Rev. B **84**, 054416 (2011).
[49] See Supplemental Material at http://link.aps.org/supplemental/10.1103/PhysRevMaterials.1.061401 for the derivation of the energy pumping in antiferromagnetic dynamics, the numerical implementation of differentiating the scattering matrix, and the details of deriving the dynamic equations of **n** and **m** including the intersublattice spin pumping.
[50] Supriyo Datta, *Electronic Transport in Mesoscopic Systems* (Cambridge University Press, Cambridge, UK, 1995).
[51] A. Kohn, A. Kovács, R. Fan, G. J. McIntyre, R. C. C. Ward, and J. P. Goff, The antiferromagnetic structures of $IrMn_3$ and their influence on exchange-bias, Sci. Rep. **3**, 2412 (2013).
[52] H. Y. Yuan, Q. Liu, K. Xia, Z. Yuan, and X. R. Wang, Proper dissipative torques in antiferromagnetic dynamics (unpublished).
[53] W. Zhang, M. B. Jungfleisch, W. Jiang, J. E. Pearson, A. Hoffmann, F. Freimuth, and Y. Mokrousov, Spin Hall Effects in Metallic Antiferromagnets, Phys. Rev. Lett. **113**, 196602 (2014).
[54] O. K. Andersen, Z. Pawlowska, and O. Jepsen, Illustration of the linear-muffin-tin-orbital tight-binding representation: Compact orbitals and charge density in Si, Phys. Rev. B **34**, 5253 (1986).
[55] Y. Liu, Z. Yuan, R. J. H. Wesselink, A. A. Starikov, M. van Schilfgaarde, and P. J. Kelly, Direct method for calculating temperature-dependent transport properties, Phys. Rev. B **91**, 220405(R) (2015).
[56] K. Xia, M. Zwierzycki, M. Talanana, P. J. Kelly, and G. E. W. Bauer, First-principles scattering matrices for spin transport, Phys. Rev. B **73**, 064420 (2006).
[57] X. Jia, K. Liu, K. Xia, and G. E. W. Bauer, Spin transfer torque on magnetic insulators, Europhys. Lett. **96**, 17005 (2011).
[58] R. Cheng, J. Xiao, Q. Niu, and A. Brataas, Spin Pumping and Spin-Transfer Torques in Antiferromagnets, Phys. Rev. Lett. **113**, 057601 (2014).
[59] Y. Y. Wang, C. Song, B. Cui, G. Y. Wang, F. Zeng, and F. Pan, Room-Temperature Perpendicular Exchange Coupling and Tunneling Anisotropic Magnetoresistance in an Antiferromagnet-Based Tunnel Junction, Phys. Rev. Lett. **109**, 137201 (2012).
[60] I. Fina, X. Marti, D. Yi, J. Liu, J. H. Chu, C. Rayan-Serrao, S. Suresha, A. B. Shick, J. Železný, T. Jungwirth, J. Fontcuberta, and R. Ramesh, Anisotropic magnetoresistance in an antiferromagnetic semiconductor, Nat. Commun. **5**, 4671 (2014).
[61] T. Moriyama, N. Matsuzaki, K.-J. Kim, I. Suzuki, T. Taniyama, and T. Ono, Sequential write-read operations in FeRh antiferromagnetic memory, Appl. Phys. Lett. **107**, 122403 (2015).
[62] T. R. McGuire and R. I. Potter, Anisotropic magnetoresistance in ferromagnetic 3*d* alloys, IEEE Trans. Magn. **11**, 1018 (1975).
[63] Y. Tserkovnyak, A. Brataas, and G. E. W. Bauer, Enhanced Gilbert Damping in Thin Ferromagnetic Films, Phys. Rev. Lett. **88**, 117601 (2002); Spin pumping and magnetization dynamics in metallic multilayers, Phys. Rev. B **66**, 224403 (2002).
[64] Y. Liu, Z. Yuan, R. J. H. Wesselink, A. A. Starikov, and P. J. Kelly, Interface Enhancement of Gilbert Damping from First Principles, Phys. Rev. Lett. **113**, 207202 (2014).
[65] J. Foros, A. Brataas, Y. Tserkovnyak, and G. E. W. Bauer, Current-induced noise and damping in nonuniform ferromagnets, Phys. Rev. B **78**, 140402 (2008).
[66] S. Zhang and S. S.-L. Zhang, Generalization of the Landau-Lifshitz-Gilbert Equation for Conducting Ferromagnets, Phys. Rev. Lett. **102**, 086601 (2009).
[67] Z. Yuan, K. M. D. Hals, Y. Liu, A. A. Starikov, A. Brataas, and P. J. Kelly, Gilbert Damping in Noncollinear Ferromagnets, Phys. Rev. Lett. **113**, 266603 (2014); H. Y. Yuan, Z. Yuan, K. Xia, and X. R. Wang, Influence of nonlocal damping on the field-driven domain wall motion, Phys. Rev. B **94**, 064415 (2016).
[68] A. Saib, *Modeling and Design of Microwave Devices Based on Ferromagnetic Nanowires* (Presses Universitaires du Louvain, Louvain-la-Neuve, Belgium, 2004).
[69] A. Kamra and W. Belzig, Spin pumping and shot noise in ferrimagnets: Bridging ferro- and antiferromagnets, Phys. Rev. Lett. **119**, 197201 (2017).